VIP 2D Nanomaterials Very Important Paper

DOI: 10.1002/anie.201405762

Nanocrystalline-Graphene-Tailored Hexagonal Boron Nitride Thin Films**

Kang Hyuck Lee, Hyeon-Jin Shin, Brijesh Kumar, Han Sol Kim, Jinyeong Lee, Ravi Bhatia, Sang-Hyeob Kim, In-Yeal Lee, Hyo Sug Lee, Gil-Ho Kim, Ji-Beom Yoo, Jae-Young Choi, and Sang-Woo Kim**

Abstract: *Unintentionally formed nanocrystalline graphene (nc-G) can act as a useful seed for the large-area synthesis of a hexagonal boron nitride (h-BN) thin film with an atomically flat surface that is comparable to that of exfoliated single-crystal h-BN. A wafer-scale dielectric h-BN thin film was successfully synthesized on a bare sapphire substrate by assistance of nc-G, which prevented structural deformations in a chemical vapor deposition process. The growth mechanism of this nc-G-tailored h-BN thin film was systematically analyzed. This approach provides a novel method for preparing high-quality two-dimensional materials on a large surface.*

Hexagonal boron nitride (h-BN) is an excellent dielectric material and may be used as a substrate for two-dimensional (2D) electronic devices.[1–8] It exploits the superior electronic properties of graphene and other 2D materials without suffering from charge traps, impurities, and charge-carrier inhomogeneity at the interface.[9,10] Atomically flat h-BN nanosheets of micrometer scale are generally produced by the micromechanical cleavage of a bulk h-BN crystal.[11] Chemical vapor deposition (CVD) has been regarded as a promising technique for the synthesis of large-scale h-BN thin films.[12–19] Although previous studies have demonstrated that an h-BN thin film could be grown on a metal substrate without impurities and BN allotropes by CVD, this thin film was not free from various structural deformations, such as ripples and wrinkles, owing to the submicrometer surface roughness of the metal catalyst and a large difference between the thermal expansion coefficients (TECs) of the metal catalyst and h-BN.[20–24]

We herein present a promising breakthrough that prevents structural deformations in CVD-grown h-BN thin films by using nanocrystalline graphene (nc-G) as the catalytic seed layer. This h-BN thin film is atomically flat and without structural deformations, and thus comparable to exfoliated h-BN. We utilized nc-G that had been unintentionally obtained by absorption of carbon by a metal catalyst as the catalytic seed layer. Furthermore, a wafer-scale ultraflat h-BN thin film was successfully synthesized on a bare sapphire substrate by assistance of nc-G. For the growth of the h-BN thin film, we employed atmospheric-pressure CVD and a borazine ($B_3N_3H_6$) precursor (see the Supporting Information). The surface roughness distribution (scan area: $5\times5\ \mu m^2$) of the grown h-BN thin film that was obtained by atomic force microscopy (AFM) is shown in Figure 1a. It was thus found that the surface of the h-BN thin film has significantly fewer wrinkles, ripples, and impurity particles. Furthermore, the surface roughness of the h-BN thin film has a root mean square (RMS) roughness value of 0.38 nm, which is comparable to that of an h-BN nanosheet exfoliated from single-crystalline bulk h-BN.[11]

To investigate the structural properties of the h-BN thin film, it was analyzed by cross-sectional high-resolution transmission electron microscopy (HRTEM). Interestingly, it was found that the thin film is composed of a long-range-ordered crystalline h-BN region (in red) and a short-range-ordered carbon region (in green; Figure 1b). High-magnification HRTEM (white box in Figure 1b) clearly indicates that the h-BN region has a well-aligned layered structure (Figure 1c). This fact was further confirmed by the fast Fourier transform (FFT) pattern of the h-BN region (Figure 1d). The interlayer distance between the h-BN layers is approximately 3.46 Å, which is almost same as that of single-crystalline bulk h-BN.[12]

Element maps that were obtained by energy-filtered TEM (EFTEM) indicated that a distinct region of boron atoms (B) and a distinct region of carbon atoms (C) exist (Figure 1e). The bright red area corresponds to the B mapping of the h-BN region, whereas the bright green area corresponds to the

[*] K. H. Lee,[+] H. S. Kim, Prof. J.-B. Yoo, Prof. S.-W. Kim
School of Advanced Materials Science and Engineering
Sungkyunkwan University (SKKU)
Suwon 440-746 (Republic of Korea)
E-mail: kimsw1@skku.edu
Dr. H.-J. Shin,[+] Dr. H. S. Lee, Dr. J.-Y. Choi
Samsung Advanced Institute of Technology
Yongin 446-712 (Republic of Korea)
E-mail: jaeyoung88.choi@samsung.com
Dr. B. Kumar
NUSNNI-NanoCore, National University of Singapore
T-Lab Level 11, 5A Engineering Drive 1, 117580 (Singapore)
J. Lee, Dr. R. Bhatia, I.-Y. Lee, Prof. G.-H. Kim, Prof. J.-B. Yoo, Prof. S.-W. Kim
SKKU Advanced Institute of Nanotechnology (SAINT)
Sungkyunkwan University (SKKU)
Suwon 440-746 (Republic of Korea)
Dr. S.-H. Kim
Electronics and Telecommunications Research Institute
Daejeon, 305-700 (Republic of Korea)
[+] These authors contributed equally to this work.

[**] This work was financially supported by the Basic Science Research Program (2012R1A2A1A01002787 and 2009-0083540) and the Global Frontier Research Center for Advanced Soft Electronics (2013M3A6A5073177) through the National Research Foundation (NRF) of Korea, which is funded by the Ministry of Science, ICT & Future Planning.

Supporting information for this article is available on the WWW under http://dx.doi.org/10.1002/anie.201405762.

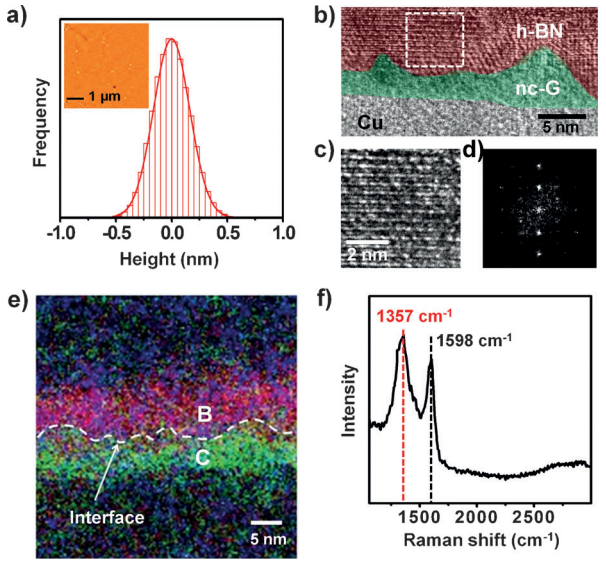

Figure 1. a) Surface roughness distribution as determined by AFM measurements and a corresponding AFM image (inset) of the h-BN thin film surface. b) Cross-sectional TEM image of the h-BN thin film. The red and green regions indicate h-BN and nc-G, respectively. c) HRTEM image of the area marked as a white box in the Figure 1 b. d) FFT pattern of the h-BN region. e) EFTEM image of the cross-sectional interface between the h-BN region and the nc-G region. f) Raman spectrum of the h-BN thin film on the nc-G-stacked structure.

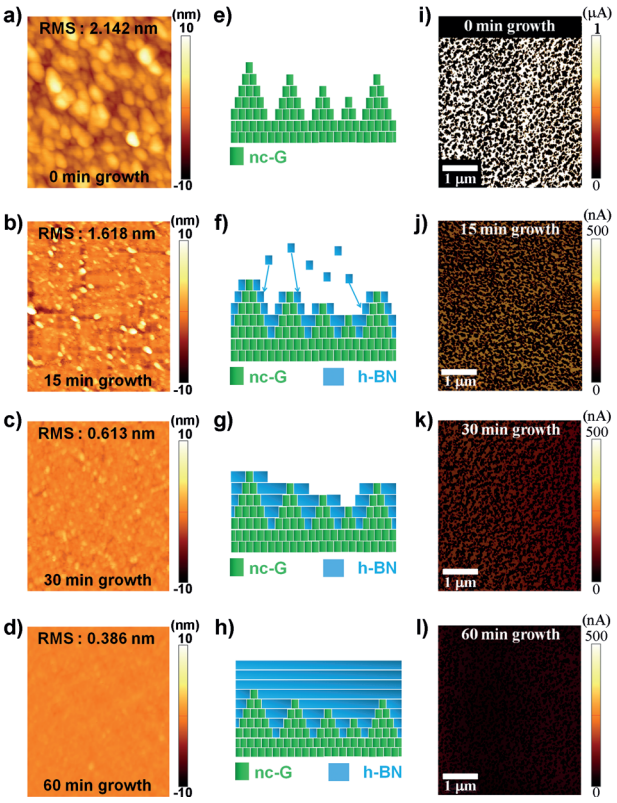

Figure 2. AFM images showing the surface morphologies of h-BN thin films grown for different periods of time: a) 0 min, b) 15 min, c) 30 min, and d) 60 min. e–f) Schematic representation of the formation mechanism of h-BN on nc-G, illustrating each growth step. The current AFM images (i–l) correspond to the AFM images (a–d).

C mapping of the carbon layer region. The element maps further confirm that crystalline h-BN was grown on the short-range-ordered carbon-stacked structure with a very rough surface morphology. In addition, two peaks are observed at 1357 and 1598 cm^{-1} in the Raman spectrum of the h-BN thin film that was grown on the nc-G-stacked structure; these peaks are similar to those observed for graphene with a D mode at 1335 cm^{-1} and a G mode at 1590 cm^{-1}. Considering that the general B–N vibration mode (E_{2g}) is located at 1367 cm^{-1}, it can be suggested that the peak at 1357 cm^{-1} is due to the superposition of the E_{2g} mode of h-BN and the G mode of graphene.[25–27] Interestingly, the nc-G-stacked structure was formed on a Cu foil without using carbon precursors at the beginning of the h-BN growth (Supporting Information, Figure S1). Raman spectroscopy, AFM, and X-ray photoelectron spectroscopy (XPS) consistently confirmed that the as-formed carbon layer is composed of nc-Gs (Figure S1 and S2).

It has previously been reported that graphene or a graphitic carbon layer can be formed on a transition-metal substrate without any carbon precursor owing to the segregation and precipitation of dissolved carbon into the metal substrate.[28] However, the maximum carbon solubility in copper is quite small (ca. 0.04 at %), thus the segregation mechanism can be ruled out for the formation of the nc-Gs in this work. Nevertheless, we confirmed that the formation of the nc-G-stacked structure on copper is reproducible under atmospheric pressure. However, at pressures below 1 Torr, it was very difficult to observe the formation of nc-Gs (Figure S3). Therefore, we suggest that nc-G formation is caused by small amounts of carbon-containing gases in air, such as methane.

The h-BN thin film exhibits an ultraflat surface morphology, whereas the nc-G film exhibits a very rough surface morphology with a RMS roughness of 2.14 nm (Figure 2 a). Furthermore, the rough interface between the h-BN region and the nc-G region suggests that nc-G plays a very important role for the lateral growth of h-BN. AFM images describe the surface morphology evolution of the h-BN thin films that were grown with the $B_3N_3H_6$ source as a function of growth time (Figure 2 a–d). After 60 minutes, the h-BN thin film exhibited a distinct ultraflat surface morphology, compared to the rough surface of the nc-G film without h-BN growth (at 0 min, Figure 2 a). The h-BN thin film obtained after growth for 90 minutes also revealed a similar flat surface morphology (Figure S4 a).

The more reactive sp^3 carbon species at the edge of nc-G (Figure 2 e) are energetically favorable sites for edge-initiated lateral growth of h-BN[29–35] owing to the relatively weak van der Waals interactions (sp^2–sp^2 interactions) between h-BN and graphene, which both feature sp^2 hybridization and a hexagonal atom arrangement. Therefore, the $B_3N_3H_6$ vapor reacts more easily with the activated edges of the nc-G owing to the lateral sp^2 growth of h-BN (Figure 2 f) followed by the formation of the flat surface. With an increase in growth time, all domains of the nc-G effectively cause the lateral growth of h-BN (Figure 2 g). As a result, an ultraflat h-BN thin film is obtained on the nc-G film (Figure 2 h). However, it was found that h-BN nanoislands with a 3D growth mode and a low

growth rate were formed on the ultraflat surface of the h-BN thin film, which led to a film with a rough surface morphology (Figure S4a). Once the ultraflat surface has been formed, only a small number of edges are available for lateral sp^2 growth of h-BN. Therefore, the additional growth of h-BN follows the 3D growth mode on the h-BN surfaces[16] (Figure S4b). A current image of the nc-G that was analyzed by AFM (Figure 2i) reveals irregular currents ranging from 1 to 1.529 μA (1 V sample bias). However, these films become more insulated for longer h-BN growth times. Finally, the optimized h-BN thin film (60 min growth, Figure 2l) has an electrically insulating surface with a current of less than 143 nA.

To confirm that the growth of ultraflat h-BN thin films can be tailored by nc-G, we studied the direct growth of h-BN on *c*-plane sapphire (c-Al_2O_3) with an nc-G layer (Figure 3a) and monolayer graphene. A h-BN thin film was perfectly formed on a two-inch c-Al_2O_3 substrate with the nc-G layer (Figure 3b). Confocal Raman mapping of the superposition of the Raman D band of nc-G and the E_{2g} vibration mode of h-BN (1335–1375 cm^{-1}) showed that the h-BN thin film had been successfully grown (Figure 3c). The Raman spectrum of the h-BN thin film that had been grown on the nc-G/c-Al_2O_3 substrate (Figure 3d) revealed the same feature as that obtained from the h-BN sample on the nc-G/Cu foil (Figure 1f). The surface of the h-BN thin film that had been grown on the c-Al_2O_3 substrate using the nc-G catalytic seed layer was atomically flat with a surface RMS roughness of 0.33 nm, which is similar to the surface RMS roughness of the h-BN thin film on the nc-G/Cu system (Figure 1a) as shown in Figure 3e. On the other hand, uniformly flat h-BN does not form on a monolayer graphene-transferred c-Al_2O_3 substrate under the equivalent growth conditions (Figure S5). This result indicates that nc-G can act as a useful seed for the growth of high-quality h-BN with an atomically flat surface on an arbitrary substrate.

Generally, 2D materials that have been grown using a metal catalyst in a CVD process contain a large number of structural deformations owing to the different TECs between the metallic catalyst and the 2D material, i.e., positive TECs for metals (TEC of Cu: $+16.5\times10^{-6}\ K^{-1}$) and negative TECs for the 2D materials (TEC of h-BN: $-2.9\times10^{-6}\ K^{-1}$).[23,24] Therefore, it can be proposed that the formation of the h-BN thin film on the nc-G-stacked structure with an ultraflat surface morphology with very few structural deformations (wrinkles or ripples) caused by thermal stress[26,27] is due to the similar negative TECs of nc-G and h-BN.

Figure 4a–c presents the XPS spectra of the h-BN thin film for boron, nitrogen, and carbon. It was previously reported that the B 1s and N 1s core levels in bulk h-BN are detected at 190.1 and 398.1 eV, respectively.[12] However, we observed that the h-BN thin film obtained in this work has two types of B 1s core-level peaks at 190.39 (B–N) and 191.81 eV (B–Ox, partial boron–oxygen bonding; Figure 4a). The N 1s peak is located at 397.97 eV (Figure 4b), which is similar to the position reported for bulk h-BN. The C 1s core level has three types of C 1s core-level peaks, which are also

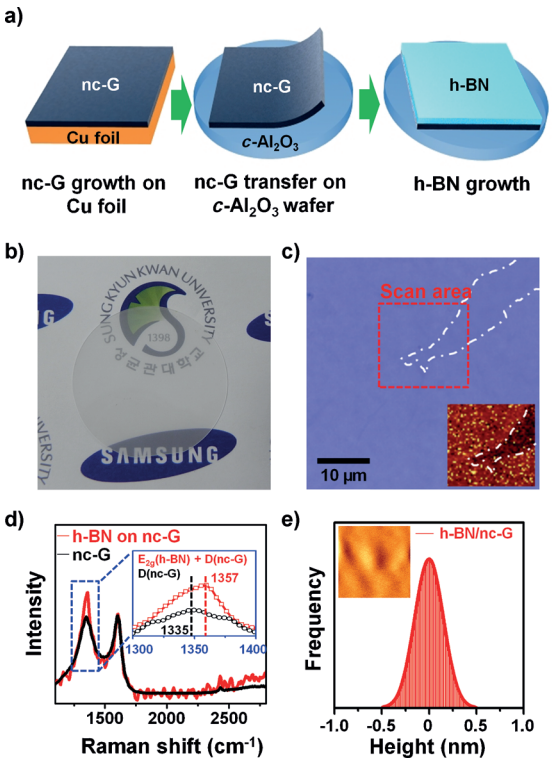

Figure 3. a) Synthesis of the h-BN thin film on a c-Al_2O_3 substrate using nc-G. b) Photograph of the wafer-scale transparent h-BN thin film grown on the two-inch c-Al_2O_3 substrate. c) Optical microscopy image and confocal Raman mapping image (inset) of the h-BN thin film on c-Al_2O_3. d) Raman spectrum of the h-BN thin film on the c-Al_2O_3 substrate. Inset: Raman spectrum at 1300–1400 cm^{-1} (D peak position). e) Histogram of the surface height distribution of the h-BN thin film.

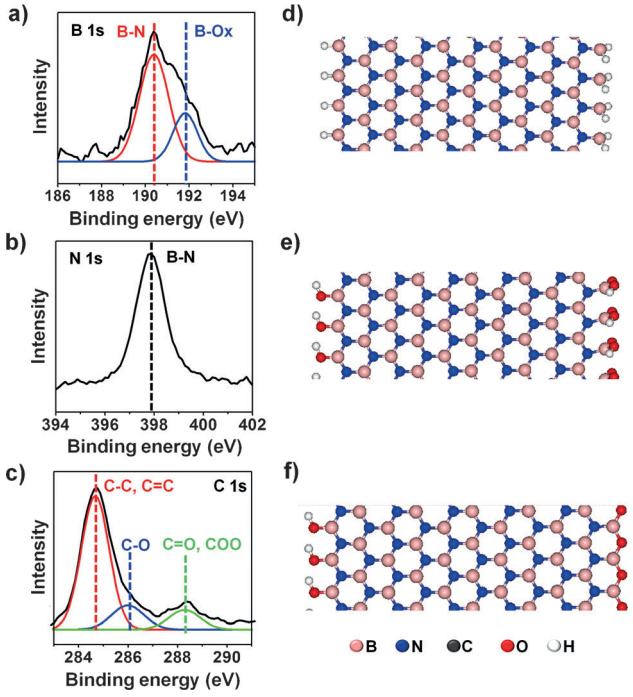

Figure 4. XPS spectra of the a) B 1s, b) N 1s, and c) C 1s core levels of the nc-G-tailored h-BN thin film. d–f) Schematic representations of the h-BN monolayers with H, OH, and OH/O terminated B edges, respectively.

observed for nc-G with no h-BN (Figure S2a) However, the intensity ratio of the C–O and C=O/COO bonds with sp^3-hybridized carbon atoms is different in the nc-G-tailored h-BN thin film (Figure 4c) and pristine nc-G. Furthermore, no B–C and N–C bonds were observed in the XPS measurements, indicating that a B–C–N phase had not been formed. Thus we suggest that the nc-G sp^3 edges are not directly connected to the h-BN sp^3 edges, and that B–O and C–O bond formation plays an important role for the lateral initiation of the growth of h-BN from the edges of nc-G.

The role of the nc-G sp^3 edges for the formation of h-BN with an atomically flat surface on the rough nc-G layer can be understood by calculating the maximum stabilization energies of h-BN monolayers terminated with B, N, O, and H atoms using the Vienna ab initio simulation package, suggesting that the h-BN monolayers have H, OH, and OH/O terminated B edges (Figure 4d–f). In a reducing atmosphere (abundant H_2), the H-terminated N edge is more stable than the H-terminated B edge. However, in ambient atmosphere, both the B and N edges have a much higher probability of O termination than of H termination. It was found that the O-terminated B edge is more stable than the O-terminated N edge. Furthermore, the OH-terminated structure is more stable than the O-terminated structure when the B edge is terminated with an O atom. A B edge terminated with OH functional groups is the most stable situation. During the formation of h-BN on nc-G, O-rich sites are mainly localized along the edges of nc-G as the chamber is kept in the reducing atmospheric condition by injection of H_2 gas and the dehydrogenation of borazine. Therefore, it can be concluded that the sp^3 edges of nc-G play a key role in the initiation and lateral growth of h-BN on the nc-G layer without any help of metal catalysts. The maximum surface stabilization energies are summarized in Table 1.

Table 1: Surface stabilization energies in h-BN monolayers.

Terminating moiety	B edge [eV]	N edge [eV]
H	1.74	2.73
OH	5.68	3.40
OH/O	4.83	2.38

In summary, it was found that an unintentionally formed nc-G acts as a useful seed for the large-area synthesis of an h-BN thin film with an atomically flat surface comparable to that of exfoliated single crystal h-BN. A wafer-scale dielectric h-BN thin film was successfully synthesized on a bare *c*-Al_2O_3 substrate by assistance of nc-G to prevent structural deformations in the CVD process. On the other hand, uniformly flat h-BN does not form on a monolayer graphene-transferred *c*-Al_2O_3 substrate under the equivalent growth conditions, indicating that the sp^3 edges of nc-G played a key role in the formation of h-BN with an atomically flat surface on the rough nc-G layer.

Received: May 30, 2014
Published online: September 9, 2014

Keywords: boron nitride · chemical vapor deposition · electron microscopy · graphene · nanostructures

[1] C. R. Dean, A. F. Young, I. Meric, C. Lee, L. Wang, S. Sorgenfrei, K. Watanabe, T. Taniguchi, P. Kim, K. L. Shepard, J. Hone, *Nat. Nanotechnol.* **2010**, *5*, 722–726.
[2] S. Mayorov, R. V. Gorbachev, S. V. Morozov, L. Britnell, R. Jalil, L. A. Ponomarenko, P. Blake, K. S. Novoselov, K. Watanabe, T. Taniguchi, A. K. Geim, *Nano Lett.* **2011**, *11*, 2396–2399.
[3] W. Gannett, W. Regan, K. Watanabe, T. Taniguchi, M. F. Crommie, A. Zettl, *Appl. Phys. Lett.* **2011**, *98*, 242105.
[4] K. F. Mak, K. He, J. Shan, T. F. Heinz, *Nat. Nanotechnol.* **2012**, *7*, 494–498.
[5] L. Britnell, R. V. Gorbachev, R. Jalil, B. D. Belle, F. Schedin, M. I. Katsnelson, L. Eaves, S. V. Morozov, A. S. Mayorov, N. M. R. Peres, A. H. Castro Neto, J. Leist, A. K. Geim, L. A. Ponomarenko, K. S. Novoselov, *Nano Lett.* **2012**, *12*, 1707–1710.
[6] K. K. Kim, A. Hsu, X. Jia, S. M. Kim, Y. Shi, M. Dresselhaus, T. Palacios, J. Kong, *ACS Nano* **2012**, *6*, 8583–8590.
[7] M. S. Choi, G.-H. Lee, Y.-J. Yu, D.-Y. Lee, S. H. Lee, P. Kim, J. Hone, W. J. Yoo, *Nat. Commun.* **2013**, *4*, 1624.
[8] M. Goossens, S. C. M. Driessen, T. A. Baart, K. Watanabe, T. Taniguchi, L. M. K. Vandersypen, *Nano Lett.* **2012**, *12*, 4656–4660.
[9] E. H. Hwang, S. Adam, S. Das Sarma, *Phys. Rev. Lett.* **2007**, *98*, 186806.
[10] J.-H. Chen, C. Jang, S. Xiao, M. Ishigami, M. S. Fuhrer, *Nat. Nanotechnol.* **2008**, *3*, 206–209.
[11] C. Lee, Q. Li, W. Kalb, X.-Z. Liu, H. Berger, R. W. Carpick, J. Hone, *Science* **2010**, *328*, 76–80.
[12] L. Song, L. Ci, H. Lu, P. B. Sorokin, C. Jin, J. Ni, A. G. Kvashnin, D. G. Kvashnin, J. Lou, B. I. Yakobson, P. M. Ajayan, *Nano Lett.* **2010**, *10*, 3209–3215.
[13] Y. Shi, C. Hamsen, X. Jia, K. K. Kim, A. Reina, M. Hofmann, A. L. Hsu, K. Zhang, H. Li, Z.-Y. Juang, M. S. Dresselhaus, L.-J. Li, J. Kong, *Nano Lett.* **2010**, *10*, 4134–4139.
[14] P. Sutter, J. Lahiri, P. Albrecht, E. Sutter, *ACS Nano* **2011**, *5*, 7303–7309.
[15] S. Chatterjee, Z. Luo, M. Acerce, D. M. Yates, A. T. C. Johnson, L. G. Sneddon, *Chem. Mater.* **2011**, *23*, 4414–4416.
[16] A. Ismach, H. Chou, D. A. Ferrer, Y. Wu, S. McDonnell, H. C. Floresca, A. Covacevich, C. Pope, R. Piner, M. J. Kim, R. M. Wallace, L. Colombo, R. S. Ruoff, *ACS Nano* **2012**, *6*, 6378–6385.
[17] K. K. Kim, A. Hsu, X. Jia, S. M. Kim, Y. Shi, M. Hofmann, D. Nezich, J. F. Rodriguez-Nieva, M. Dresselhaus, T. Palacios, J. Kong, *Nano Lett.* **2012**, *12*, 161–166.
[18] P. Sutter, J. Lahiri, P. Zahl, B. Wang, E. Sutter, *Nano Lett.* **2013**, *13*, 276–281.
[19] G. Kim, A.-R. Jang, H. Y. Jeong, Z. Lee, D. J. Kang, H. S. Shin, *Nano Lett.* **2013**, *13*, 1834–1839.
[20] K. H. Lee, H.-J. Shin, J. Lee, I.-Y. Lee, G.-H. Kim, J.-Y. Choi, S.-W. Kim, *Nano Lett.* **2012**, *12*, 714–718.
[21] W. Bao, F. Miao, Z. Chen, H. Zhang, W. Jang, C. Dames, C. N. Lau, *Nat. Nanotechnol.* **2009**, *4*, 562–566.
[22] D. Yoon, Y.-W. Son, H. Cheong, *Nano Lett.* **2011**, *11*, 3227–3231.
[23] B. Yates, M. J. Overy, O. Pirgon, *Philos. Mag.* **1975**, *32*, 847–857.
[24] W. Paszkowicz, J. B. Pelka, M. Knapp, T. Szyszko, S. Podsiadlo, *Appl. Phys. A* **2002**, *75*, 431–435.
[25] P. K. Chu, L. Li, *Mater. Chem. Phys.* **2006**, *96*, 253–277.
[26] L. Ci, L. Song, C. Jin, D. Jariwala, D. Wu, Y. Li, A. Srivastava, Z. F. Wang, K. Storr, L. Balicas, F. Liu, P. M. Ajayan, *Nat. Mater.* **2010**, *9*, 430–435.
[27] Z. Liu, L. Song, S. Zhao, J. Huang, L. Ma, J. Zhang, J. Lou, P. M. Ajayan, *Nano Lett.* **2011**, *11*, 2032–2037.

[28] N. Liu, L. Fu, B. Dai, K. Yan, X. Liu, R. Zhao, Y. Zhang, Z. Liu, *Nano Lett.* **2011**, *11*, 297 – 303.
[29] Y.-H. Lee, X.-Q. Zhang, W. Zhang, M.-T. Chang, C.-T. Lin, K.-D. Chang, Y.-C. Yu, J. T.-W. Wang, C.-S. Chang, L.-J. Li, T.-W. Lin, *Adv. Mater.* **2012**, *24*, 2320 – 2325.
[30] P. Sutter, R. Cortes, J. Lahiri, E. Sutter, *Nano Lett.* **2012**, *12*, 4869 – 4874.
[31] M. P. Levendorf, C.-J. Kim, L. Brown, P. Y. Huang, R. W. Havener, D. A. Muller, J. Park, *Nature* **2012**, *488*, 627 – 632.
[32] S. M. Kim, A. Hsu, P. T. Araujo, Y.-H. Lee, T. Palacios, M. Dresselhaus, J.-C. Idrobo, K. K. Kim, J. Kong, *Nano Lett.* **2013**, *13*, 933 – 941.
[33] Y. Gao, Y. Zhang, P. Chen, Y. Li, M. Liu, T. Gao, D. Ma, Y. Chen, Z. Cheng, X. Qiu, W. Duan, Z. Liu, *Nano Lett.* **2013**, *13*, 3439 – 3443.
[34] Z. Liu, L. Ma, G. Shi, W. Zhou, Y. Gong, S. Lei, X. Yang, J. Zhang, J. Yu, K. P. Hackenberg, A. Babakhani, J.-C. Idrobo, R. Vajtai, J. Lou, P. M. Ajayan, *Nat. Nanotechnol.* **2013**, *8*, 119 – 124.
[35] Z. Sun, T. Liao, Y. Dou, S. M. Hwang, M.-S. Park, L. Jiang, J. H. Kim, S. X. Dou, *Nat. Commun.* **2014**, *5*, 3813.

